Enhancing Post-Punching Performance of Flat Plate-Column Joints by Different Reinforcement Configurations

Youzhe Yang[a], Yi Li[a*], Hong Guan[b], Mengzhu Diao[b], Xinzheng Lu[c]

[a] Beijing Key Laboratory of Earthquake Engineering and Structural Retrofit, Beijing University of Technology, Beijing 100124, China.

[b] School of Engineering and Built Environment, Griffith University Gold Coast Campus, Queensland 4222, Australia.

[c] Key Laboratory of Civil Engineering Safety and Durability of Ministry of Education, Tsinghua University, Beijing 100084, China.

Abstract: To enhance post-punching strengths and deformation capacities of flat plate-column joints for mitigating progressive collapse, two strengthening methods including stirrups and embedded ring beams within the joint regions were proposed. An experimental test program on six flat plate-column joint specimens with in-plane constraints was conducted under the modes of upward punching shear failure (UPS mode) and downward punching shear failure (DPS mode). The specimens included two conventional specimens without strengthening (UPS/DPS), two specimens with stirrups (two-legged closed ties, UPS-S/DPS-S) and two specimens with ring beams (UPS-R/DPS-R). The test results showed that, in comparison to UPS/DPS, the average post-punching displacements in UPS-S/DPS-S and UPS-R/DPS-R were increased by 25% and 32%, respectively, along with 64% and 50% enhancement in the corresponding post-punching shear strengths. Numerical simulations were also performed to analyze the effects of different stirrup and ring beam configurations on the post-punching strengths and deformation capacities. Numerical results suggested that double stirrups (four-legged closed ties) installed surrounding the column stub could lessen joint damage and further improve punching shear and

* Corresponding author, Email: yili@bjut.edu.cn

post-punching strengths by 15% and 9%, respectively, comparing to UPS-S/DPS-S. For ring beam specimens, under DPS mode, the first punching shear failure inside the ring beams can be prevented by their inner edges directly connected to the column. The post-punching deformations and strengths of this specimen were increased by at least 10%, comparing to DPS-R. Numerical simulation of UPS-R further showed that the strengthening effect also depends on the constraints provided by the concrete.

Keywords: Flat plate-column joints, post-punching performance, reinforcement strengthening configuration, stirrups, embedded ring beams

1 Introduction

Flat plate structures are a type of reinforced concrete (RC) structures in which the floor is directly supported by the column. Flat plate-column joints in these structures are prone to brittle punching shear failure, resulting in their lower ductility and load resistance compared to frame structures. In addition, without beams to transfer loads, limited load redistribution paths are provided in flat plate structural systems. Accordingly, once an initial local failure caused by various accidental events (e.g., overload, explosion, fire, etc.) occurred, it is more likely to trigger progressive collapse of the overall structural system. Given the catastrophic consequences of the progressive collapse events of RC flat plate structures, e.g., the collapses of Sampoong department store [1], Gretzenbach parking [2] and Skyline Plaza [3], etc., progressive collapse prevention strategies for flat plate structures have been the focus of study in academic and professional communities [4-8]. In the process of progressive collapse, flat plate-column joints undergo three distinctive stages: bending action under small deformations, punching shear failure, and suspension action under large deformations [9]. After punching shear failure, the joints can still provide a certain level of post-punching strength under large deformations, through tensile forces developed in reinforcing bars going through the columns, thereby contributing to progressive collapse prevention of the entire flat plate structures. There have been a large number of studies on the mechanism of punching shear failure under small deformations [10-14]. However, research on the post-punching mechanism of flat plate-column joints under large deformations is relatively scarce. More importantly, current design guidelines for preventing

progressive collapse and corresponding strengthening methods are mostly for steel and concrete frames, whereas the robustness design regulations for RC flat plate structures are much needed [15-17].

Due to the inherent brittleness of punching shear failure of a flat plate-column joint, its load-resistant capacity may not be readily and effectively improved by simply optimizing its structural parameters (such as slab thickness, concrete strength, reinforcement ratio, etc.). With this in mind, researchers have conducted extensive experimental and theoretical studies aimed at improving punching shear strengths of these joints, by adopting high strength concrete [18], or installing shear components such as shear studs [19-22], bent-up reinforcements [23], prestress tendons [24], and shear stirrups [25]. These strengthening methods have been confirmed to be able to improve the punching shear strengths and deformation capacities of joints by providing additional shear transferring ability and added benefit of confining concrete and limiting crack propagation.

Existing strengthening methods were aimed at improving the punching shear strength and deformation of the joints under small deformations. For progressive collapse research, attention must also be paid on the post-punching strengths of the joints under large deformations, which can make a significant impact on the failure propagation resulted from an initial local damage. Relevant research in this area is however limited. For instance, Faria et al. [26] proposed a strengthening system in which the post-tensioning steel strands were bonded to the concrete slab using epoxy adhesive. Such a method increased the post-punching strength of the joint by 78% relative to the punching shear strength. However, the existing laboratory tests followed the same setup for punching shear tests, in which the joint specimens were simply supported along the slab edges and in-plane constraints of the surrounding slabs to the joints were neglected. As a result, the contribution of compressive membrane action of concrete under small deformations was not taken into consideration [27]. In addition, tensile membrane action can only be mobilized through reinforcing bars going through the punching cracks at large-deformation suspension stage with sufficient in-plane constraints. Without which, the post-punching strength of the joint specimens might be underestimated. To address such an experimental limitation, Diao et al. [28] performed four joint tests with in-plane constraints to investigate the punching and post-

punching failure mechanisms of slab-column joints with variations of embedded beams. It was observed that the punching strength of the specimen with embedded beams was 15% higher than that of the conventional specimen. Confinement provided by the stirrups within the embedded beams enabled synchronized deformations of slab longitudinal rebars. Consequently, the post-punching resistance and the corresponding displacement were increased by 97% and 37%, respectively.

Stirrups could be a simple and effective alternative to enhance both punching and post-punching resistance and deformation capacities of flat plate-column joints. To be specific, the punching strength of the joints is dominated by the quantity of stirrups going through the punching cracks, whereas the post-punching strength is regulated by the number of longitudinal reinforcements confined by stirrups [28]. Ring beams have been widely used in concrete-filled steel-tube composite structures to improve the seismic performance of the frame joints. Research outcomes [29-31] indicated that ring-beam connection systems are effective in improving seismic resistance because the joints are confined thereby having adequate strength and cyclic stiffness. The concept of stirrups and embedded ring beams could also be applied to flat plate-column joint areas, by which necessary confinement to the concrete can be provided thereby improving the post-punching strength of the joints. These reinforcement configurations are also practically advantageous in which they can effectively increase the load resistance of the joints for progressive collapse prevention, whilst do not require any extra device and are efficient in installation and low in cost.

Two failure modes can both trigger progressive collapse of a flat plate structure, namely, downward punching shear failure (referred to as DPS) and upward punching shear failure (referred to as UPS). The mechanical behaviors of the flat plate-column joints with and without strengthening may be distinguishably different under opposite punching directions [28]. To gain an in-depth understanding of the post-punching performance of flat plate-column joints strengthened by stirrups and embedded ring beams under two different failure modes, an experimental test program was conducted on six joint specimens, including two conventional specimens without strengthening, two specimens with stirrups (two-legged closed ties), and two specimens with embedded ring beams. Three-dimensional (3D) nonlinear finite-element models

were also created using LS-DYNA, by which the post-punching strengths and deformations of the specimens were analyzed. Based on the experimental tests and numerical simulations, most effective configurations of stirrups and ring beams for performance-based optimum design of flat plate-column joints were suggested.

2 The experimental program

The prototype structure is a 4×4-bay, 6,000 mm column spacing flat plate office structure, illustrated in Fig. 1, which was designed in accordance with both AS 3600 [32] and GB50010 [33]. Note that the two adjacent middle spans of length l=6,000mm would become a single span of double length L=2l after the middle column was damaged by accidental events (Fig. 1a), making the contra-flexure point to be 0.56l away from the removed middle column (i.e., l-0.22×2l) [34]. The tested joint specimen of 6,000 mm × 6,000 mm in size was extracted from the ground floor of the prototype structure (Fig. 1b), at a 3,000 mm distance from the removed middle column, approximately matching with the location of contra-flexure. A scaled ratio of 1/3 was chosen for the tested specimens, and the slab dimension of which was 2,000 × 2,000 mm, the slab thickness was 90 mm, the concrete cover was 6 mm, the cross-section and the height of column stub at the slab center were 150 × 150 mm and 300 mm, respectively.

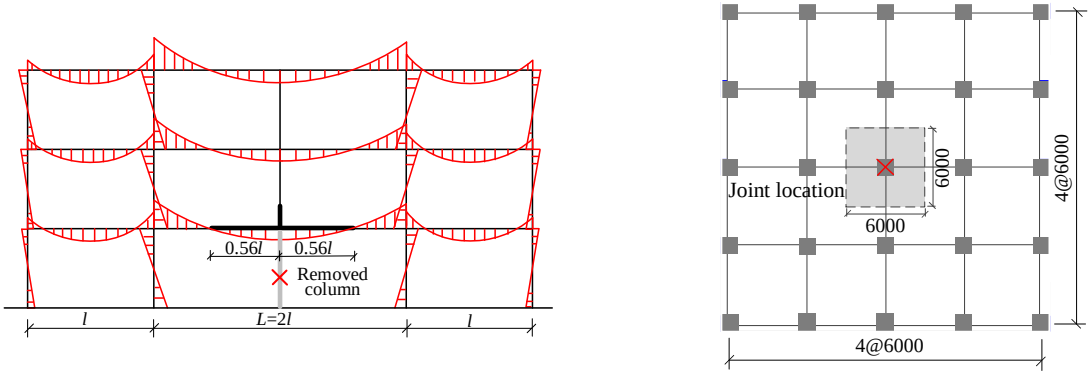

(a) (b)

Fig. 1 Plan view of the prototype structure (units: mm)

The slab edges of specimens were cast together with large-sized boundary beams [28] (Fig. 2), to replicate the in-plane constraints provided by the surrounding slabs in real buildings. While the DPS specimens had their continuous integrity reinforcements (IRs) and flexural reinforcements (FRs) placed at the slab bottom and top, respectively, like in the actual structure, the UPS

specimens had a reversed arrangement of IRs and FRs (Figs. 3 and 4). Also in the UPS specimens, IRs at the slab top were bent down at the slab-boundary beam interface and were further extended into the boundary beams, to achieve the same boundary condition as in the DPS specimens. To be specific, under small deformations, bending restraints were released at the onset of tensile cracking at the top slab surface; and subsequently under large deformations, in-plane tensile restraints were provided to the longitudinal reinforcements (IRs and FRs). It is noted that once the size and the amount of reinforcements of the boundary beams were large enough to enable sufficient in-plane constraints to the joint specimen, further strengthening the boundary beams was unnecessary as additional enhancement of the constraints was trivial. A pilot test was conducted firstly to confirm the feasibility and reliability of the required constraints provided by the boundary beams. Tests of all the six specimens further indicated that the maximum horizontal displacement of the boundary beams was 5 mm, being only 1/400 the span length of 2,000 mm. According to the deflection limit of 1/250 the span length in AS 3600, the designed boundary beams have been confirmed to remain in the elastic stage during the course of tests whilst providing effective in-plane restraints.

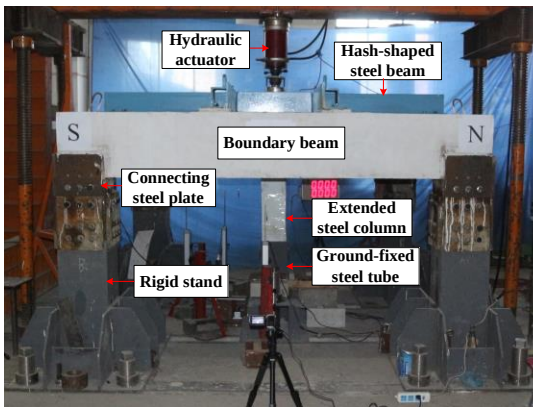

Fig. 2 Test setup

The boundary beams of the specimens were connected to four rigid stands (see Fig. 2). The construction detailing of boundary beams are shown in Fig. 5. To avoid twisting and tilting of the column stub during the loading process, the stub was inserted into a ground-fixed, square steel tube underneath the column. Polytetrafluoroethylene (PTFE) was smeared on the inner surface of the steel tube to reduce friction and allow smooth vertical displacement of the column stub inside the steel tube. The reaction force of the column was measured by the load cell mounted at the tip of the hydraulic jack. Two linear variable displacement transducers (LVDTs) were placed at the

south and north faces of the removed column stub, and another transducer was installed on one side of the boundary beams to monitor the horizontal displacement. Strains developed in the reinforcing bars were measured by strain gauges glued to the reinforcements at critical locations (Figs. 3 and 4). A quasi-static loading scheme was adopted and a downward displacement was applied to the column stub by a hydraulic actuator, until the joints underwent large deformations in the post-punching stage and its load resistant capacity was completely exhausted, for investigating the mechanical behavior of the joints.

To provide an insight into the collapse-resistant mechanisms of RC flat plate-column joints influenced by the proposed strengthening methods, six experimental tests of the conventional joint specimens (UPS/DPS) and those strengthened by stirrups in the punching area (UPS-S/DPS-S) and by embedded ring beams (UPS-R/DPS-R) were conducted. In UPS-S/DPS-S, four sets of 6-row stirrups were installed parallel to each side of the column. As for UPS-R/DPS-R, ring beams consisted of rebars forming the inner and outer rings and four sets of 4-row stirrups perpendicular to each side of the column. The reinforcement details of the specimens are summarized in Table 1 and illustrated Figs. 3 and 4. Material properties of the specimens are given in Table 2. Reinforcement detailing of UPS/DPS reported in the published paper [28] was consistent with that of UPS-S/DPS-S and UPS-R/DPS-R, but without the strengthening reinforcements.

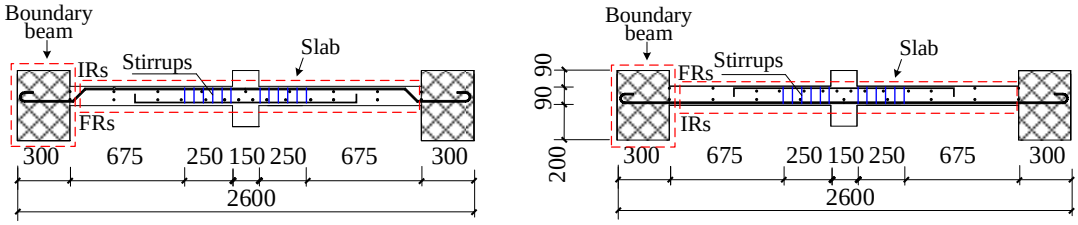

(a) UPS-S

(b) DPS-S

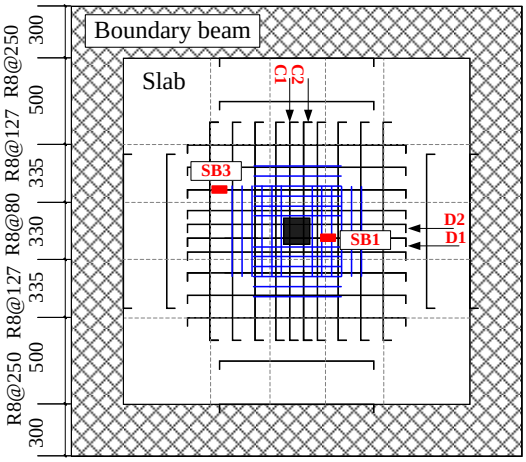

Note: Blue lines represent four sets of 6-row stirrups (two-legged closed ties) parallel to each side of column; C1/C2 and D1/D2 represent FRs in UPS specimens; SB1/3 represent strain gauges in UPS and UPS-S.

(c) Flexural reinforcement (FR)

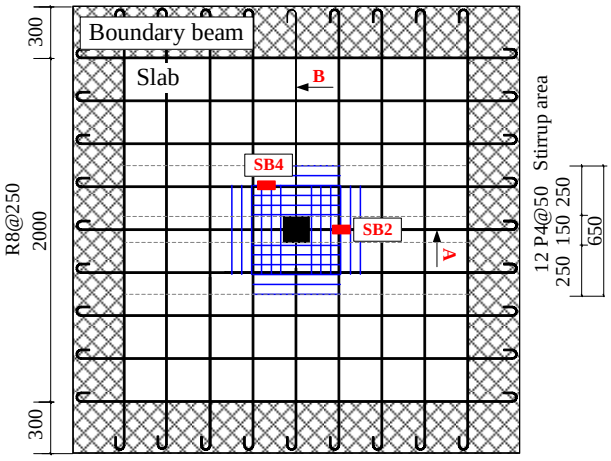

Note: A and B represent IRs in UPS specimens; SB2/4 represent strain gauges in DPS and DPS-S.

(d) Integrity reinforcement (IR)

Fig. 3 Reinforcements in UPS-S and DPS-S (unit: mm)

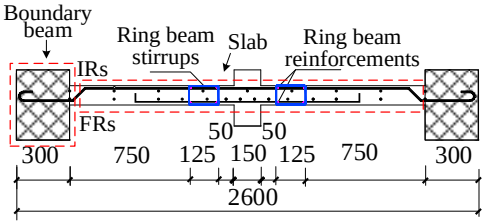

(a) UPS-R

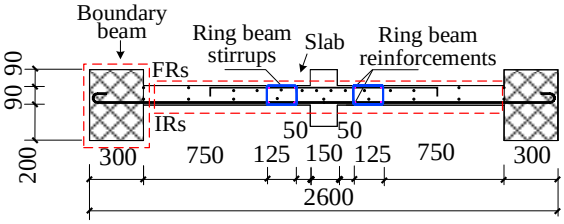

(b) DPS-R

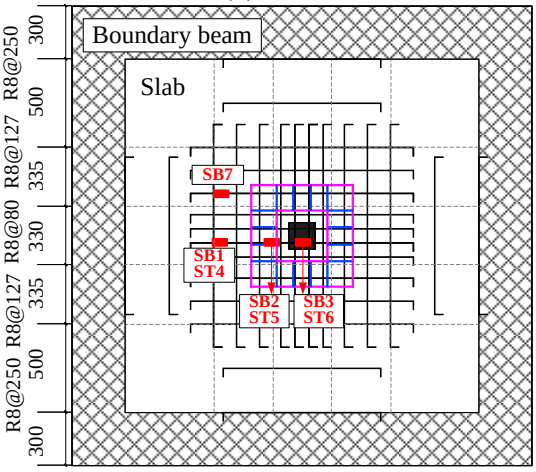

Note: Pink rings represent boundary of ring beams; blue lines represent four sets of 4-row stirrups perpendicular to each side of column forming ring beams; SB1-SB3, SB7 and ST4-ST6 represent strain gauges in UPS-R (slab bottom) and DPS-R (slab top), respectively.

(c) Flexural reinforcement (FR)

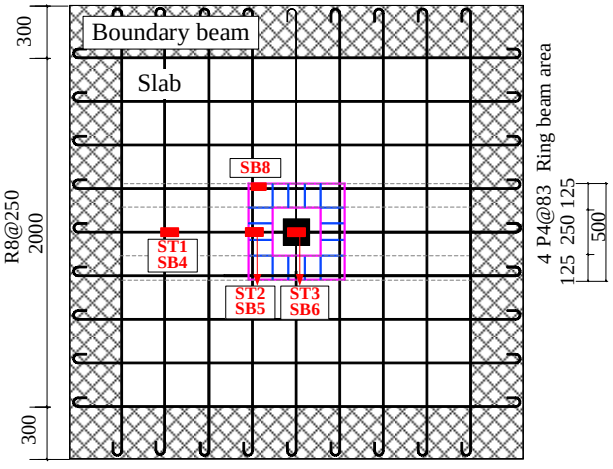

Note: ST1-ST3 and SB4-SB6, SB8 represent strain gauges in UPS-R (slab top) and DPS-R (slab bottom), respectively.

(d) Integrity reinforcement (IR)

Fig. 4 Reinforcement in UPS-R and DPS-R (unit: mm)

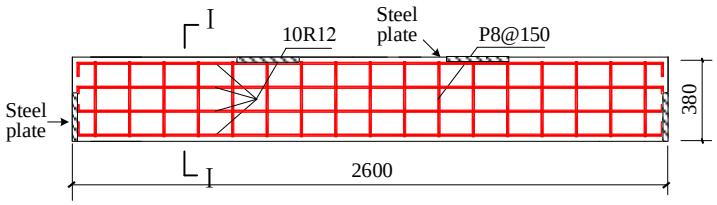

(a) Reinforcement in boundary beam (front view)

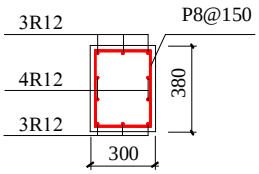

(b) Reinforcement in boundary beam (I-I section)

Fig. 5 Reinforcement in boundary beams

Table 1 Reinforcements in slab (unit: mm)

Specimens	Integrity reinforcement (IR)			Flexural reinforcement (FR)		
	Column strip (s/2)		Middle strip (s/2)	Column strip (s/2)		Middle strip (s/2)
	$c \le b+2h$	$c > b+2h$		$c \le b+2h$	$c > b+2h$	
UPS/DPS	R8@250	R8@250	R8@250	R8@80	R8@127	R8@250
UPS-S/DPS-S	R8@250	R8@250	R8@250	R8@80	R8@127	R8@250
UPS-R/DPS-R	R8@250	R8@250	R8@250	R8@80	R8@127	R8@250

Note: s is the centre-to-centre spacing between columns, c is the width of column/middle strip, b is the column width, h is the slab thickness. b+2h refer to Clause 9.1.2 in AS 3600 [32].

Table 2 Material properties of specimens

	Type	f_y (MPa)	f_u (MPa)	E_s (GPa)	e (%)
Steel	P4	667	734	196	5
	P8	298	471	205	29
	R8	436	643	205	24
	R12	511	608	215	15

	Specimens	f_c (MPa)	Specimens	f_c (MPa)
Concrete	UPS	27.2	DPS	27.2
	UPS-S	24.3	DPS-S	24.4
	UPS-R	22.5	DPS-R	30.8

Note: f_y, f_u, E_s and e are the yield strength, ultimate strength, elastic modulus and ratio of elongation of steel bars, respectively, f_c is the compressive cylinder strength of concrete. "P" and "R" represent the hot-rolled plain bars and hot-rolled ribbed bars, respectively.

3. Test results and discussions

3.1 Conventional specimens UPS/DPS

The test results of the conventional joints (UPS and DPS) were only briefly presented here, for the purpose of comparison with the newly proposed enhanced joint specimens. The details of the test results can be found in the published paper [28]. The load-displacement curves of UPS/DPS are shown in Fig. 6. The deflection and the load applied to the column stub are denoted by Δ and

F, respectively. Points F_p、F_t、F_{pp} denote, respectively, the punching shear strength, the residual strength at punching to post-punching mechanism transition and the peak load at the suspension stage (post-punching strength), which are also highlighted on the load-displacement curves.

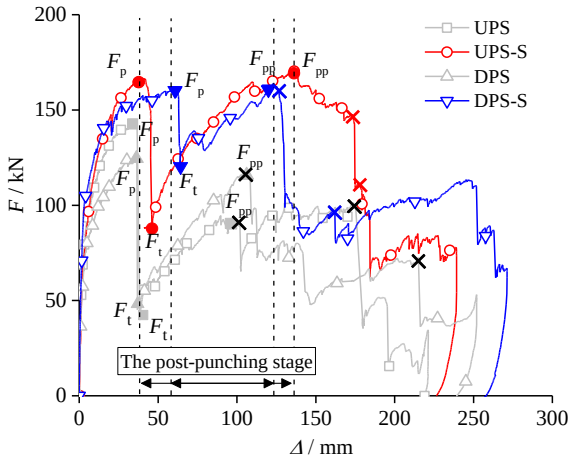

Note: × represents reinforcement rupture

Fig. 6 Load-displacement curves of UPS/DPS and UPS-S/DPS-S

Typical observations of the UPS and DPS specimen during the entire loading process up to ultimate failure are concrete cracking at the slab bottom, punching shear failure of the joints (F_p), rupture of the top rebars going through the column (F_{pp}), pull-out and rupture of the bottom rebars. The opposite observations between UPS and DPS specimens are: in UPS specimen, damage occurred in the following sequencing: rupture of the top rebars (IRs), pull-out of the bottom rebars (FRs) from the slab soffit, and rupture of FRs going through the column. However, DPS specimen demonstrated a different sequencing: fracture of FRs, pull-out of IRs, and rupture of IRs going through the column.

Before punching shear failure, the applied load was transferred through the bending mechanism of the slab, hence the load resistance and deformation of the joint were governed by the composite action of concrete and reinforcing bars. In the UPS specimen, the top IRs and bottom FRs in the vicinity of the column stub resisted the load by compressive and tensile actions, respectively, and vice versa in the DPS specimen. As the quantity of bottom FRs in UPS was 36% larger than the bottom IRs in DPS, UPS exhibited lager flexural resistant capacity, which resulted in a 16% higher punching shear strength than that of DPS.

After punching shear failure, further deformation led to rapid damage of the concrete at the punching cone, and the applied load was resisted and transferred in the form of tensile forces within the longitudinal reinforcements passing through the punching cracks. Note that the load applied to the top of the column stub was firstly transferred to the reinforcing bars going through the column; then through the contact of the reinforcement net, the load was passed onto the peripheral rebars; and ultimately the load was evenly distributed to the slab. Following this load transfer path, post-punching strengths and deformations of UPS and DPS were governed by the reinforcing bars going through the column. With increased joint deformations after punching shear failure, the resistance of the joints rose steadily until the first rupture of a rebar. Thereafter, the concrete in the close vicinity of the column damaged severely and unable to provide necessary confinement to the reinforcing bars, which could no longer offer much resistance to the applied load. For this reason, the load-displacement phase from punching shear failure to reinforcement rupture was considered to be a steady post-punching stage. Throughout this stage, top reinforcements being very close to the loading point and better confined by the large portion of the concrete, therefore experienced larger rotation ($\alpha > \beta$) and contributed more to the load resistance, comparing to those of the bottom reinforcements (shown in Fig. 7a). The fact that the amount of top FRs in DPS was larger than that of top IRs in UPS has led to 26% and 17% higher resistance and stiffness (calculated by $(F_{pp}\text{-}F_t)/(\Delta_{pp}\text{-}\Delta_t)$) of DPS than those of UPS, respectively.

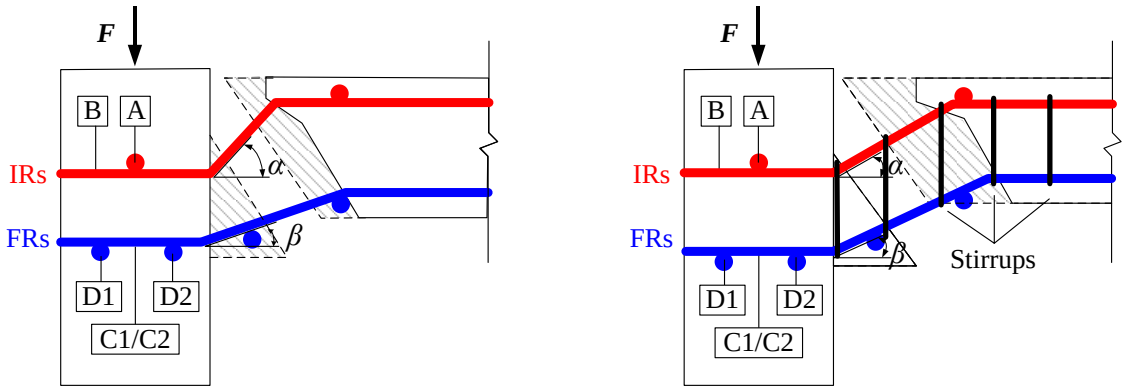

(a) UPS (b) UPS-S

Fig. 7 Post-punching mechanisms of UPS specimens

3.2 Specimens strengthened by stirrups UPS-S/DPS-S

The load-displacement curves of UPS-S/DPS-S are also presented in Fig. 6. Evidently, stirrups significantly improved the mechanical behavior of the joints throughout the process of pre- and

post-punching shear failure. Before punching shear failure, stirrups provided not only shear resistance directly but also confinement to larger area of concrete, which consequently contributed to the overall shear resistance. As a result, both punching strengths and deformation capacities of the UPS-S and DPS-S specimens were largely improved. Punching strengths of UPS-S and DPS-S (i.e., F_p) were 15% and 29% higher than those of UPS and DPS, respectively. The corresponding punching deformations were increased by 11% and 67% in UPS-S and DPS-S, respectively. Moreover, stirrups enabled more slab reinforcements to participate in resisting the applied load, hence the load drop after punching was reduced. The residual capacities (F_t) at the mechanism transition were 123% and 177% higher in UPS-S and DPS-S, comparing to those in UPS and DPS, respectively.

After punching shear failure, the concrete within the punching cone remained integrity owing to the confinement of stirrups. In addition, more peripheral rebars surrounding the column also resisted the load together with the through-column rebars. Hence, while in UPS/DPS there was a large difference in the strain patterns between through-column rebars and peripheral reinforcements (Fig. 8), the strain patterns in UPS-S/DPS-S rebars were very similar (as illustrated in Fig. 9). Fig. 7b illustrates the post-punching mechanism of the joint specimen with stirrups, using UPS-S as an example. The rotations of reinforcements at the slab top (α) and bottom (β) were almost the same before the specimen reaching the peak strength F_{pp}, due to the integrity of concrete and the contribution of more peripheral reinforcements. This can be confirmed by the simulation results (Section 4) indicating smaller differences in the average angles and the tensile strengths among the four rebar layers going through the column in UPS-S and DPS-S (8° and 61MPa, respectively), relative to the larger values in UPS and DPS (16° and 249MPa, respectively). These factors leaded to that rupture of rebars going through the column was delayed and the post-punching resistance was increased in UPS-S and DPS-S. To be specific, the post-punching deformations (i.e., Δ_{pp}) in UPS-S and DPS-S were 13% and 36% larger than those in UPS and DPS, respectively, and the corresponding resistances (i.e., F_{pp}) were increased by 86% and 41%, respectively.

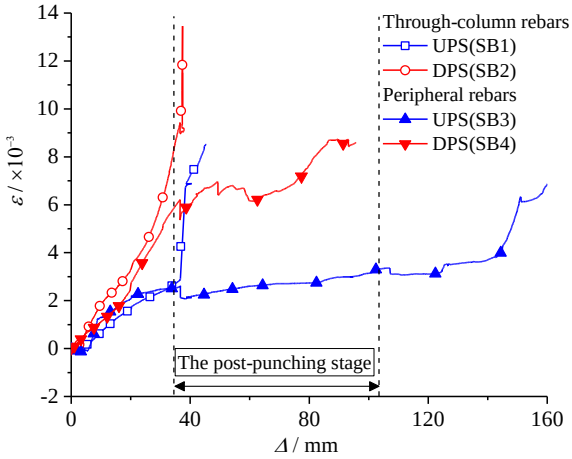

Fig. 8 Reinforcement strains in UPS and DPS

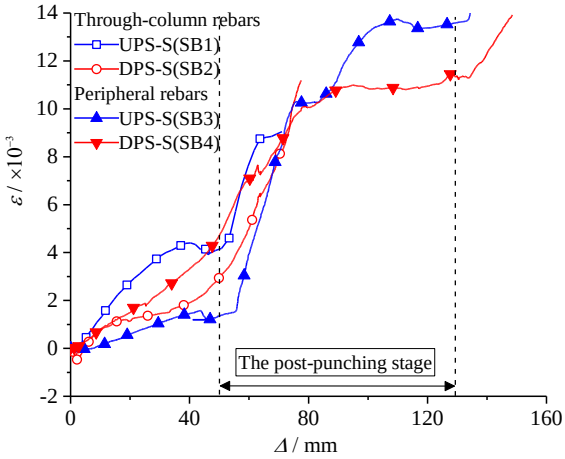

Fig. 9 Reinforcement strains in UPS-S and DPS-S

The damage patterns of UPS-S and DPS-S were also different from those of UPS and DPS. To be specific, punching shear failure observed in UPS-S and DPS-S were not as severe as those in UPS and DPS. At the post-punching peak load (i.e., F_{pp}), reinforcing bars going through the column fractured in UPS and DPS. However, no reinforcements in UPS-S and DPS-S ruptured at F_{pp}, because the concrete and longitudinal reinforcements were better confined by the stirrups, leading to uniform growth of the strain in reinforcements (Fig. 9). Also, at F_{pp}, UPS-S and DPS-S experienced critical shear failure of the concrete core, resulting in a drop in the load resistance. After that, the reinforcements going through the column ruptured almost at the same time in UPS-S and DPS-S; whereas successive rupture of the same reinforcements in UPS and DPS were witnessed (rupture of reinforcement was marked in Fig. 6).

In the UPS and DPS specimens, the average post-punching strength (i.e., F_{pp}) was 22% lower than the average punching strength (i.e., F_p). On the other hand, the average F_{pp} in UPS-S and DPS-S was 3% higher than the average F_p. This implies that the stirrups increased the post-punching residual resistance of the joints, which was more conducive to progressive collapse preventing of flat plate structures. It should be noted that the differences between UPS-S and DPS-S in terms of damage patterns, load resistances and deformations became smaller, attributable to the stirrup confinement.

3.3 Specimens strengthened by embedded ring beams UPS-R/DPS-R

The load-displacement curves of UPS-R and DPS-R, shown in Fig. 10, indicate that there are three fluctuations of load resistance. The first and second fluctuations were resulted from local punching shear failure happened on the inner and outer sides of the ring beams, respectively. The third one was caused by rupture of reinforcing bars going through the column and fracture of the stirrups in UPS-R and DPS-R, respectively. Confinement of the ring beams enabled the concrete and reinforcing bars to resist the applied load collaboratively, thereby shifting the original punching shear failure surface to the inner and outer edges of the ring beams. Test results show that, although some punching failures occurred exterior to the ring beam region, confinement effects have increased the deformation capacity (i.e., Δ_{p1}) and the punching strength (i.e., F_{p1}) of DPS-R by 36% and 23%, respectively, comparing to those of DPS. Discreteness of the concrete material used in UPS-R made its strength 27% lower than that of DPS-R, resulting in an earlier punching shear failure at the inner side of the ring beams in UPS-R, and decreased Δ_{p1} and F_{p1}. Having longitudinal reinforcements and stirrups within the ring beams, the total amount of rebars was increased in both specimens, which was effective to limit the sudden drop of resistance at the onset of punching shear failure. Similarly, to UPS-S and DPS-S, the values of F_{t1} of UPS-R and DPS-R were increased by 125% and 154% (Fig. 10), comparing to those of UPS and DPS, respectively.

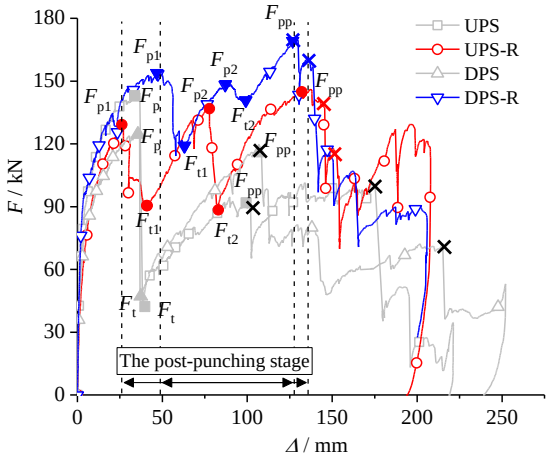

Note: × represents reinforcement rupture

Fig. 10 Load-displacement curves of UPS/DPS and UPS-R/DPS-R

In UPS-R and DPS-R, longitudinal reinforcements and stirrups within the ring beams provide necessary confinement to the rebars going through the column and those peripheral reinforcements surrounding the column, facilitating more reinforcement to resist the applied load.

Therefore, F_{pp} in UPS-R and DPS-R had 53% and 47% increases, comparing to those in UPS and DPS, respectively. In addition, confinement of the ring beams enhanced the load transfer capacity from the through-column rebars to the peripheral reinforcements surrounding the column. The combined contributions of these rebars allowed more effective resistance to the applied load. The strain data are crucial to explore the post-punching mechanisms of various joints before and after strengthening. By comparing the strain development of peripheral rebars in UPS-R/DPS-R to UPS/DPS (Fig. 11), it was found that the strains developed much faster in UPS-R/DPS-R at post-punching stage. Hence, the large deformations and resistances were perceived in the joints with ring beams due to the confinement of stirrups and ring beams.

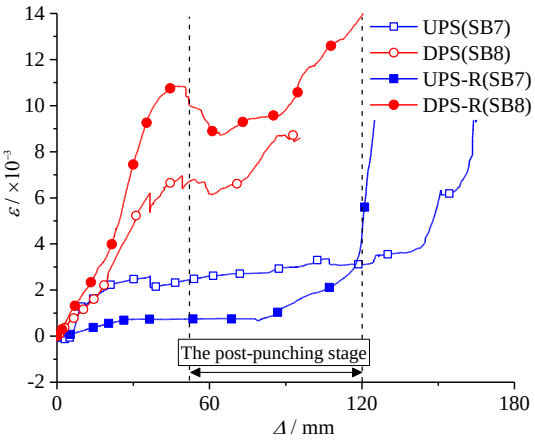

Fig. 11 Strains in peripheral reinforcements surrounding the column

In view of the load transfer paths in UPS-R and DPS-R, their post-punching strengths were regulated by the critical reinforcements going through the column, similar to UPS and DPS. As shown in Fig. 12, the reinforcement strains at the same top and bottom slab locations in UPS-R and DPS-R developed in similar trends, owing to the combined efforts of the reinforcements within the slab and ring beams. Further, the confinement effects of stirrups within the ring beams facilitated the reinforcements going through the column to deform compatibly, hence resulting in larger rotation angles and post-punching strengths. The simulation results discussed in Section 4 confirmed that the differences in the rotation angles and the tensile strengths among the four rebar layers going through the column were smaller in UPS-R and DPS-R (11° and 42MPa, respectively), in contrast to those in UPS and DPS (16° and 249MPa, respectively). Similar to the

UPS-S and DPS-S specimens, UPS-R and DPS-R also had their reinforcing bars ruptured (marked in Fig. 10) one after the other.

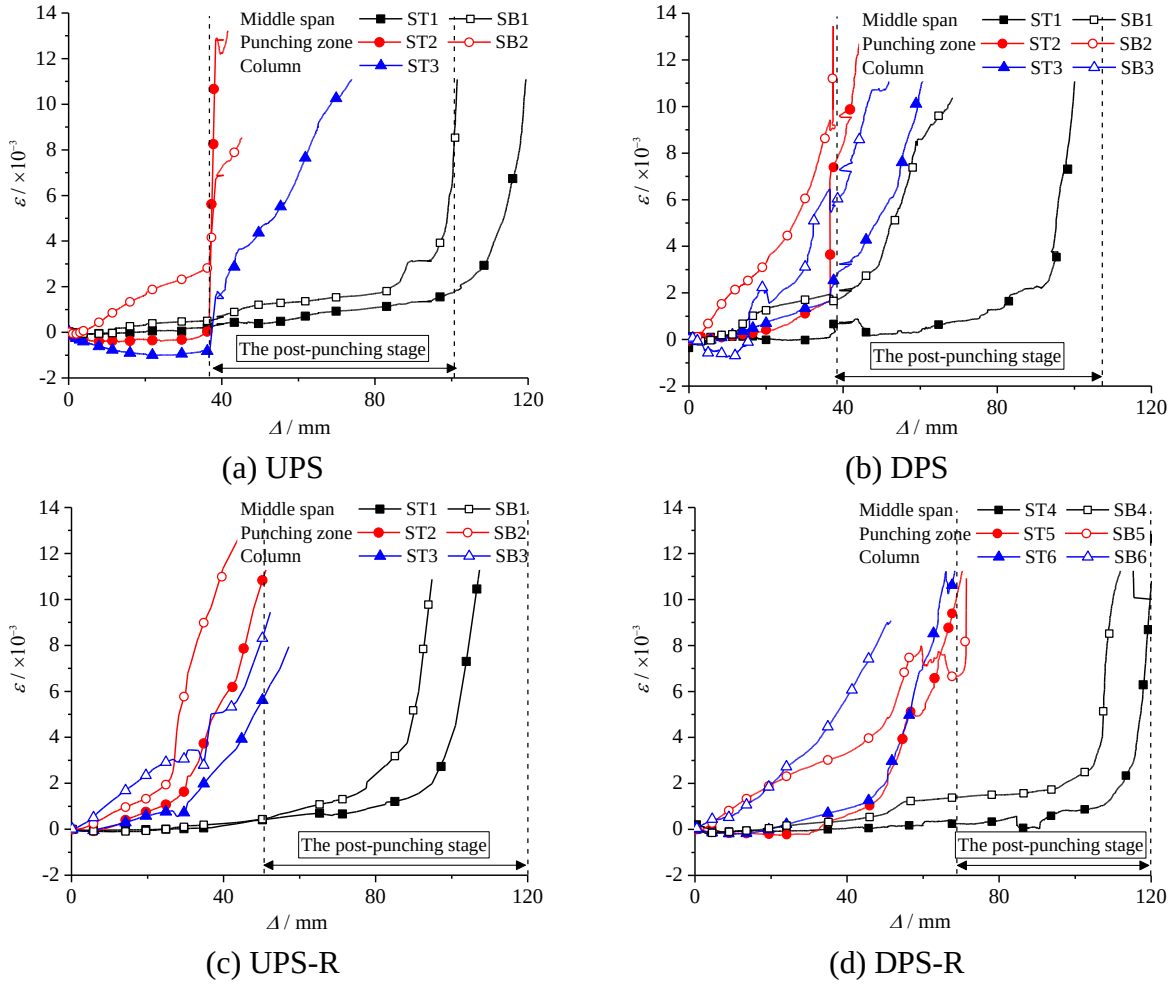

Fig. 12 Strains in through-column reinforcements

3.4 Comparison of two strengthening configurations

The failure modes of three UPS specimens with (UPS-S and UPS-R) and without (UPS) strengthening are compared in Fig. 13. Under large deformations, the UPS column stub was attached to the surrounding slabs by the slab longitudinal reinforcements only. Both UPS-S and UPS-R, on the other hand, had their surrounding slabs better involved in load carrying, in turn alleviating the degree of damage of the joint area. The structural resistances are controlled by the compressive action of concrete and tensile action of reinforcing bars. Firstly, the average diameter of the punching shear cones in UPS-S/DPS-S and UPS-R/DPS-R is approximately 90

mm, and that in UPS/DPS is 55 mm. Secondly, in Figs. 8, 9, and 11 the strains in the peripheral reinforcements in the -S (strain gages: SB3 and SB4) and -R (strain gages: SB7 and SB8) specimens were found to increase rapidly and were generally larger than the corresponding ones in UPS and DPS. Based on these observations, the enhancement configurations in the strengthening specimens enabled more slab reinforcements to participate in resisting the applied loads. Table 3 compares the displacements and the corresponding load resistances at the critical points on the load-displacement curves of all the specimens. Generally, at the punching shear failure stage, the improvements in ductility and load resistance in UPS-R and DPS-R were not as significant as those in UPS-S and DPS-S. This is mainly due to the larger-sized stirrups in UPS-S and DPS-S providing considerable shear resistant capacities. Yet, punching shear failure happened twice in UPS-R and DPS-R, leading to limited increases in their Δ_p and F_p.

(a) UPS (b) UPS-S (c) UPS-R

Fig. 13 Failure modes of UPS specimens with and without strengthening

Table 3 Displacements and the corresponding strengths at critical points

Specimens	Δ_p (mm)	F_p (kN) and percentage change		Δ_t (mm)	F_t (kN) and percentage change		Δ_{pp} (mm)	F_{pp} (kN) and percentage change	
UPS	36	144		38	40		99	92	
DPS	36	125		37	45		108	116	
UPS-S	40	166	+15.3%	46	89	+122.5	135	171	+85.9%
DPS-S	60	161	+28.8%	64	125	+177.8%	123	164	+41.3%
UPS-R	27 (78)	127 (138)	-7.9%	40 (83)	90 (87)	+121.3%	142	141	+53.3%
DPS-R	49 (88)	154 (148)	+20.8%	60 (98)	114 (140)	+182.2%	130	170	+46.6%

Note: Δ_p, Δ_t, Δ_{pp} denote the displacements corresponding to punching shear strength F_p, load resistance at mechanism transition F_t, post-punching peak load F_{pp}, respectively. Numbers in brackets are the values corresponding to the second punching-like load drop (F_{p2} in Fig. 9) in UPS-R/DPS-R. "+"and "-" represent the percentage increase and decrease in strength compared to UPS/DPS, respectively.

Post-punching deformation capacity (i.e., Δ_{pp}) and load resistance (i.e., F_{pp}) are critical indicators for evaluating the collapse-resistant performance of flat plate structures. Compared to UPS and

DPS, the average values of Δ_{pp} were increased by 25% and 32% in UPS-S/DPS-S and UPS-R/DPS-R, respectively, and the corresponding F_{pp} were increased by 64% and 50%, respectively. Considering these two indicators, installing stirrups and embedded ring beams at the punching area were both very effective to improve the deformation capacities and load resistances of the joints under large deformations. The area enveloped by a load-displacement curve represents the energy dissipation capacity of a structure in preventing a vertical collapse, and this capacity can be approximatively calculated by connecting the key points on the curve with straight lines. The average dissipation capacities of UPS-S/DPS-S and UPS-R/DPS-R were increased by 99% and 102%, respectively, comparing to those of UPS and DPS. As such, the proposed two strengthening methods have been proven to considerably enhance the collapse-resistant capacities of the joints.

4. Numerical simulation

4.1 Modelling techniques

4.1.1 Element types

To establish finite element models of the joints, eight-node 3D solid Lagrangian elements were used to simulate the concrete, along with the reduced integration algorithm (one integration point at the element center) and TYPE 1 viscous hourglass control method, by which high computational efficiency was achieved with minimized non-physical element distortions. Reinforcing bars were modelled by two-node Hughes-Liu beam elements with 2 × 2 Gauss quadrature integration across sections. This type of beam element allowed the co-existing behaviors of axial force, biaxial bending and transverse shear to be considered, to effectively replicate the large deformation of steel bars going through the concrete cracks after punching [35]. By virtue of symmetry, only 1/4 of each specimen was modelled (a typical UPS model is shown in Fig. 14), and the column, slab, boundary beam, as well as the reinforcing bars were modelled to their actual sizes and positions. A trial analysis was conducted to reach the following findings: 1) the element sizes of concrete and reinforcement were dimensioned to 15mm and 18mm, respectively, as further refinement induced high computational cost while having little impact on improving accuracy, 2) identical simulation results were obtained by the 1/4 model and the full model.

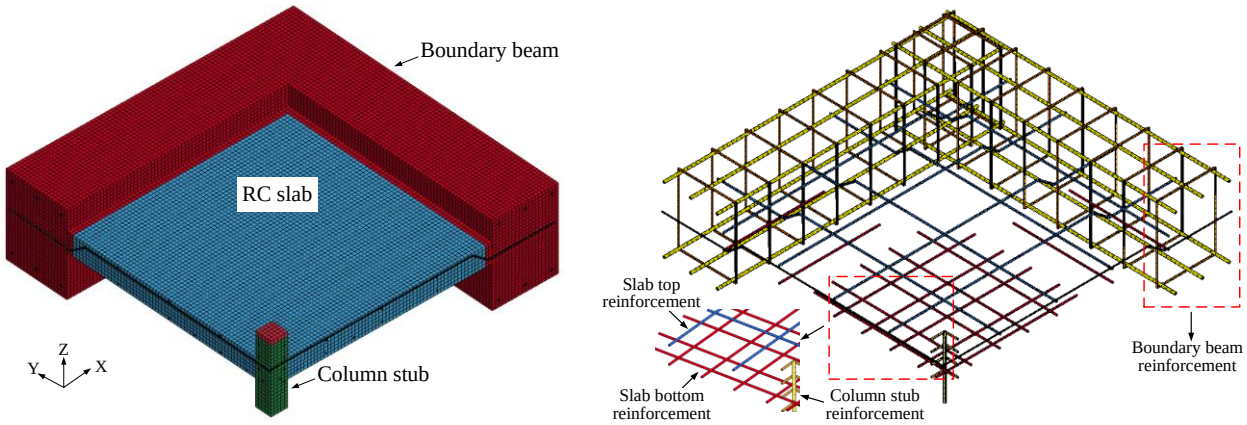

(a) 3D elements for concrete (b) Beam elements for reinforcing bars

Fig. 14 UPS model

4.1.2 Material models

Continuous surface cap model (*MAT_159/*MAT_CSCM) was adopted to define the material property of concrete. This material model enables the confinement effects and post-peak softening characteristics of concrete to be properly captured, hence being commonly used in simulating RC structures under large-deformation collapse scenarios [35-41]. In particular, the model can appropriately simulate the tensile and shear behaviors under limited lateral pressure, therefore it is highly suitable for reproducing the punching shear failure of RC slab-column joints. The elastic bulk modulus K and the shear modulus G of the concrete were calculated using the Poisson's ratio γ and the elastic modulus E recommended by CEB-FIP model [42]. The material parameters in the plastic stage were determined by the unconfined compressive strength, aggregate size and element size. The CSCM model adopts a sophisticated formulation to combine the shear failure surface with the hardening compaction surface, to smooth out the concrete constitutive curve and ensure the solution convergence when the concrete approaches the failure strain. The input values required by the CSCM model for concrete materials have been provided in Appendix 1. Fig. 15 presents the skeleton curve of unconfined uniaxial concrete with a cylinder compressive strength of 27MPa. The reinforcement material was simulated by the uniaxial, multilinear elasto-plastic material model (*MAT_024/*MAT_PIECEWISE_LINEAR_PLASTICITY). The elastic stage of steel was defined using Young's modulus and the plastic stage was determined through engineering stress-strain curves obtained from the uniaxial tensile test. The strain rate effect was neglected in the modelling of joints, as the experimental load was applied quasi-statically.

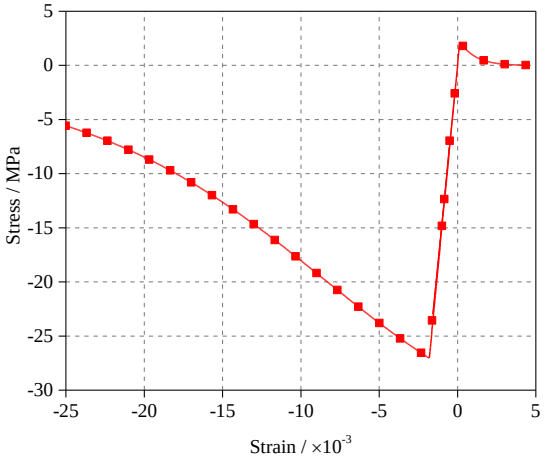

Fig. 15 Uniaxial stress-strain relationship of CSCM model

4.1.3 Constraints and failure criteria

Outside the punching area, the concrete and reinforcing bars exhibited small deformations as an integrated whole, therefore bond-slip between them can be neglected and the keyword *CONSTRAINED_BEAM_IN_SOLID was taken to completely couple the degrees of freedom of reinforcing bars and concrete. To simulate the severe crushing and spalling of concrete at the punching area, the element deletion function was activated by the keyword *MAT_ADD_EROSION if the element strain reaches the pre-defined threshold value [35-38]. Punching shear cracks are largely caused by the shear failure of concrete. In the S- and R-series specimens with stirrups, the areas in the close vicinity to the column damaged severely. Consequently, in these specimens, the maximum shear strain (i.e., $\gamma_{c,max}$) was adopted to be the failure criterion for the concrete at the punching area. Whereas for concrete in the other areas, potential shear failure, tension cracking and spalling may be co-existing, therefore the maximum effective strain (i.e., $\bar{\varepsilon}_{c,max}$) was taken to be the concrete failure criterion. Rupture of reinforcement was simulated by setting the maximum effective strain (i.e., $\bar{\varepsilon}_{c,max}$) as the failure criterion. Note that punching and post-punching mechanical behaviors are relevant to the assumed material failure criteria, and it is challenging to suggest a unified failure criterion suitable for all the test specimens due to the discreteness of the materials. For this reason, a trial and error method was used to determine the appropriate strain values ($\gamma_{c,max}$ and $\bar{\varepsilon}_{c,max}$) for the concrete, which were also calibrated against the experimental failure modes. The specific values

of the failure criteria $\gamma_{c,max}$ and $\bar{\varepsilon}_{c,max}$ for concrete and reinforcing bars have also been provided below each load-deflection comparison curves. Similar method was also used by Pham et al. in determining the concrete failure strain [36].

Subsequent to severe damage to the concrete, the applied load was mainly resisted by the reinforcing bars undergoing large deformations, and the load transfer path was influenced by the contact interaction of different rebar layers. Such a contact was defined by the keyword *CONTACT_AUTOMATIC_GENERAL together with a zero friction coefficient. This contact algorithm represents a single-surface contact, without a need to define the contact and target surfaces on the beam elements. Surface penetration can be checked by automatically examining the outer surfaces of the elements along the beam direction. Using this keyword, only the normal contact forces were considered between different layers of rebar elements without any penetration, so that the true interaction between the slab reinforcements under the large-deformation suspension stage could be realistically simulated.

The four rigid stands in the experiments were simulated by adding the lateral and bottom restraints to the concrete solid elements located at the four corners of the boundary beams. To apply a downward displacement to the top of the column stub whilst minimizing stress concentration at the loading point, a rigid body, which was only allowed to translate vertically, was created on top of the stub. The load resistance of the joint was then determined by obtaining the equivalent reaction force of the rigid body, using the keywords *DATA_CROSS_SECTION_SET and *DATABASE_SECFORC.

4.2 Numerical model validation

The experimental and predicted load-displacement curves are compared in Fig. 16 for all the six specimens. It can be seen that the load dropped dramatically at the onset of punching shear failure (i.e., F_t) in the simulation, caused by the excessive number of concrete element deletion in the vicinity of the column stub. Such is more evident for the UPS-S/DPS-S and UPS-R/DPS-R specimens having larger quantities of reinforcing bars, leading to more significant shear failure in concrete. During the post-punching stage, the load resistant capacity was mainly provided through the tensile mechanism of the slab longitudinal reinforcements. As the bonding between

the concrete and rebars were weakened, the impact of further concrete element deletion on the overall structural behavior was also reduced. Hence after the mechanism transition point (i.e., F_t), the predicted post-punching resistances correlated reasonably well with the experimental ones. The experimental and predicted displacements and the corresponding punching and post-punching strengths in Table 4. It is worthwhile mentioning that, the punching and post-punching peak strengths are the critical factors to consider in engineering design, and good agreements were achieved with a maximum deviation between the numerical and experimental peak strengths of up to 14% (Table 4). Considering large deformation analyses, such a deviation is considered acceptable. As illustrated in Fig. 17, and typically for UPS, UPS-S, UPS-R, it can be observed that the experimental post-punching failure modes of the joints can be well predicted, including severe concrete spalling, excessively deformed rebars, punching shear failure around the column stub, as well as cracks forming two circular rings at the slab bottom.

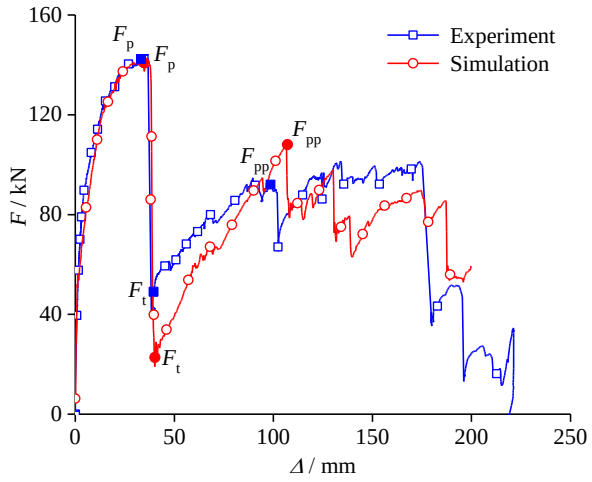

(a) UPS

(concrete: $\gamma_{c,max}$=0.022; rebar: $\bar{\varepsilon}_{c,max}$=0.079)

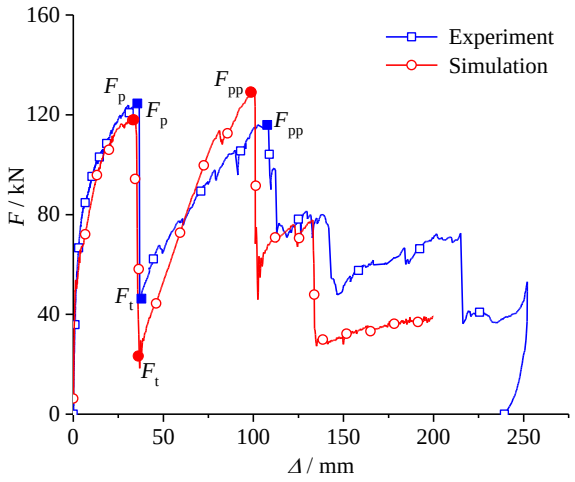

(b) DPS

(concrete: $\gamma_{c,max}$=0.02, rebar: $\bar{\varepsilon}_{c,max}$=0.083)

Note: In UPS and DPS, $\gamma_{c,max}$ was adopted to be the concrete failure criterion for the entire slab.

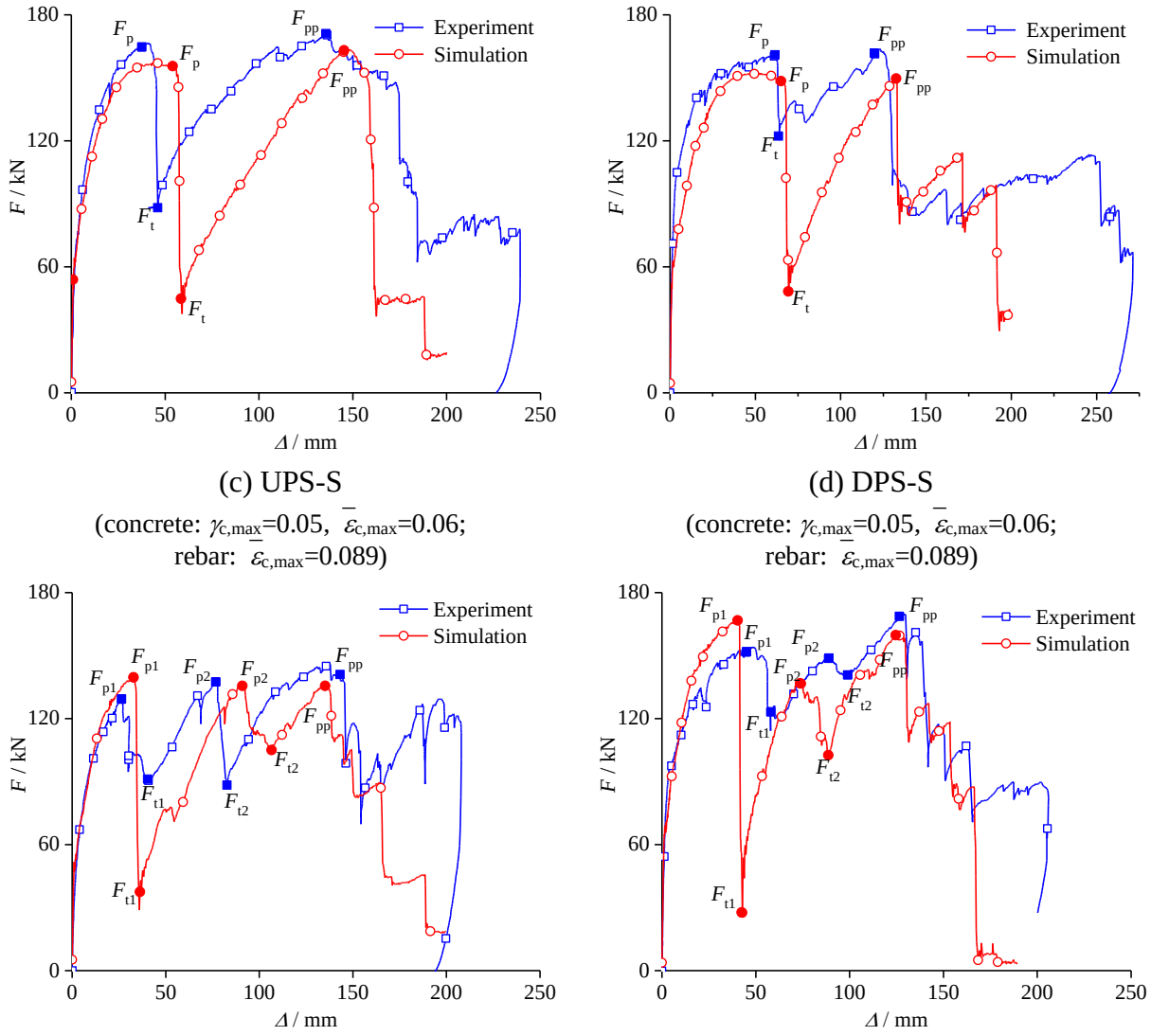

(c) UPS-S

(concrete: $\gamma_{c,max}$=0.05, $\bar{\varepsilon}_{c,max}$=0.06; rebar: $\bar{\varepsilon}_{c,max}$=0.089)

(d) DPS-S

(concrete: $\gamma_{c,max}$=0.05, $\bar{\varepsilon}_{c,max}$=0.06; rebar: $\bar{\varepsilon}_{c,max}$=0.089)

(e) UPS-R

(concrete: $\gamma_{c,max}$=0.025, $\bar{\varepsilon}_{c,max}$=0.06; rebar: $\bar{\varepsilon}_{c,max}$=0.088)

(f) DPS-R

(concrete: $\gamma_{c,max}$=0.022, $\bar{\varepsilon}_{c,max}$=0.06; rebar: $\bar{\varepsilon}_{c,max}$=0.088)

Fig. 16 Comparison of experimental and predicted load-displacement responses for all specimens

Table 4 Comparison of the experimental and predicted displacement and punching/post-punching strengths

Specimen	Punching						Post-punching					
	Experiment		Simulation				Experiment		Simulation			
	$\Delta_{p,e}$ (mm)	$F_{p,e}$ (kN)	$\Delta_{p,s}$ (mm)	$F_{p,s}$ (kN)	$\Delta_{p,s}/\Delta_{p,e}$	$F_{p,s}/F_{p,e}$	$\Delta_{pp,e}$ (mm)	$F_{pp,e}$ (kN)	$\Delta_{pp,s}$ (mm)	$F_{pp,s}$ (kN)	$\Delta_{pp,s}/\Delta_{pp,e}$	$F_{pp,s}/F_{pp,e}$
UPS	36	144	38	140	1.06	0.97	99	92	106	109	1.07	1.18
DPS	36	124	33	117	0.92	0.94	108	116	101	128	0.94	1.10
UPS-S	42	167	54	159	1.29	0.95	136	170	148	163	1.09	0.96

DPS-S	61	160	64	150	1.05	0.94	125	164	133	149	1.06	0.91
UPS-R	27(78)	127(138)	32(90)	139(135)	1.17	1.04	142	141	134	135	1.07	1.11
DPS-R	49(88)	154(148)	39(73)	166(137)	0.81	1	130	170	127	160	0.98	0.94
Deviation					14%	4%					6%	10%

Note: $\Delta_{p,e}$ and $\Delta_{pp,e}$ are the measured displacements corresponding to the experimental punching shear and post-punching strengths $F_{p,e}$ and $F_{pp,e}$, respectively; $\Delta_{p,s}$ and $\Delta_{pp,s}$ are the predicted displacements corresponding to the predicted punching shear and post-punching strengths $F_{p,s}$ and $F_{pp,s}$, respectively.

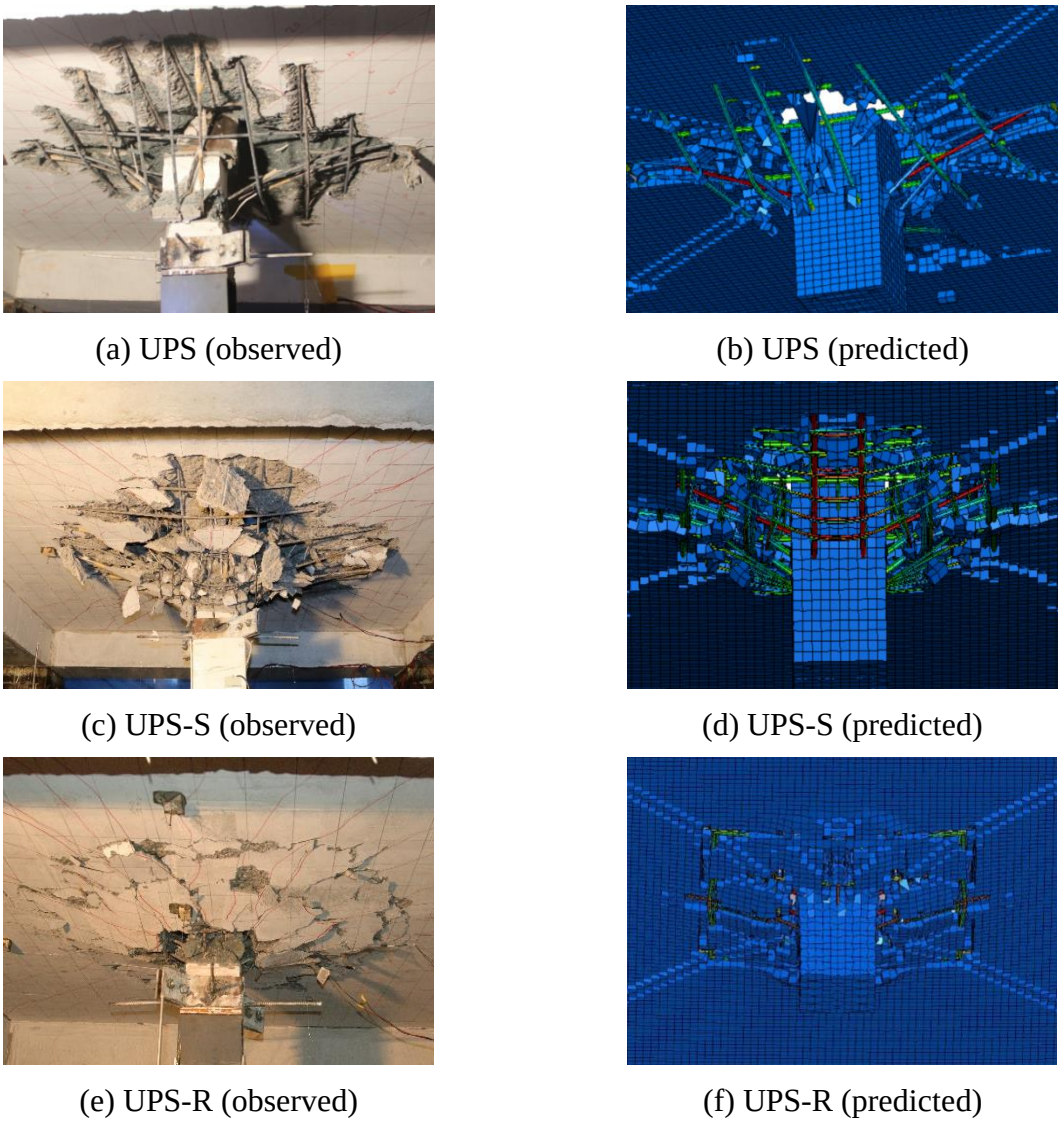

(a) UPS (observed) (b) UPS (predicted)

(c) UPS-S (observed) (d) UPS-S (predicted)

(e) UPS-R (observed) (f) UPS-R (predicted)

Fig. 17 Experimental and simulated failure modes of all specimens

Table 5 summarizes the rotational angles (α_i and β_i, i=1, 2) and the tensile strength (f_{st}, f_{sb}) of through-column rebars in the post-punching stage, based on the predicted post-punching peak load and the corresponding displacement in the same stage. For the UPS-S/DPS-S and UPS-

R/DPS-R specimens, the variations of α_i, β_i, and f_{st} of those four rebar layers are relatively less compared to those in the UPS/DPS specimens, same as the experimental observations. This again demonstrates that the stirrups and ring beams facilitate the slab reinforcing bars to carry the load and to deform more uniformly.

Table 5 Angle and strength of reinforcements passing through the column

	Slab top (IRs)				Slab bottom (FRs)			
	Upper layer		Lower layer		Upper layer		Lower layer	
	α_1(°)	$f_{st,u}$(MPa)	α_2(°)	$f_{st,l}$(MPa)	β_1(°)	$f_{sb,u}$(MPa)	β_2(°)	$f_{sb,l}$(MPa)
UPS	21	577	18	577	28	295	14	555
UPS-S	27	597	22	621	28	645	26	597
UPS-R	31	670	20	636	31	643	25	666
	Slab top (FRs)				Slab bottom (IRs)			
	Upper layer		Lower layer		Upper layer		Lower layer	
	α_1(°)	$f_{st,u}$(MPa)	α_2(°)	$f_{st,l}$(MPa)	β_1(°)	$f_{sb,u}$(MPa)	β_2(°)	$f_{sb,l}$(MPa)
DPS	29	637	22	567	12	422	11	498
DPS-S	29	631	19	597	25	605	24	557
DPS-R	32	674	21	625	28	659	28	640

Note: α_1 and α_2 are the predicted rotational angles of upper and lower rebar layers of slab top, respectively, at post-punching stage (F_{pp}), and the corresponding rebar strengths are $f_{st,u}$ and $f_{st,l}$, respectively. β_1 and β_2 are the predicted rotational angles of upper and lower rebar layers of slab bottom, respectively, at post-punching stage (F_{pp}), and the corresponding rebar strengths are $f_{sb,u}$ and $f_{sb,l}$, respectively.

5. Parametric analysis of reinforcement strengthening configurations

Flat plate-column joint specimens strengthened with stirrups and ring beams have been experimentally proven to be efficient reinforcement configurations for progressive collapse prevention of flat plate structures. Given limited laboratory tests and experimental results, numerical parametric studies were conducted to gain further insight into the effects of these two strengthening methods on the overall structural behaviors of the joints.

5.1 Effects of stirrups

To evaluate the effects of stirrups on punching and post-punching failure mechanisms of the joints, various stirrup layouts and quantities were designed based on UPS-S and DPS-S, with the aim of increasing the amount of longitudinal reinforcements and the volume of concrete confined

by the stirrups. This results in ten new joint models being designated as UPS-SI and DPS-SI (I=1 to 5). Details of these models are presented in Table 6 and Fig. 18.

(1) UPS-S1/DPS-S1: based on UPS-S/DPS-S, the quantity and length of stirrups remained unchanged, but their diameter was increased form 4 mm to 6 mm, equivalent to a 125% increase in the stirrup ratio (Fig. 18a);

(2) UPS-S2/DPS-S2: based on UPS-S/DPS-S, the quantity of stirrups remained unchanged, but their length was increased from 450 mm to 1020 mm, equivalent to an increased region covered by the stirrups (Fig. 18b);

(3) UPS-S3/DPS-S3: based on UPS-S2/DPS-S2, the stirrup ratio was increased by 50% through adding more stirrups (Fig. 18c);

(4) UPS-S4/DPS-S4: based on UPS-S2/DPS-S2, internal stirrups (red colored lines) were added to create four-legged closed ties (Fig. 18d);

(5) UPS-S5/DPS-S5: based on UPS-S3/DPS-S3, internal stirrups (red colored lines) were added to create four-legged closed ties (Fig. 18e).

Table 6 Numerical parametric models with different layout and quantity of stirrups

Specimen	d_b (mm)	n	s (mm)	l (mm)
UPS-S1/DPS-S1	P6	12	50	650
UPS-S2/DPS-S2	P4	12	70	1020
UPS-S3/DPS-S3	P4	18	50	1020
UPS-S4/DPS-S4	P4	12 (12)	70	1020
UPS-S5/DPS-S5	P4	18 (18)	50	1020

Note: d_b is the stirrup diameter, n is the number of stirrups, s in the stirrup spacing, l is the covering length of stirrups. Numbers in bracket are the number of internal stirrups in four-legged closed ties specimens.

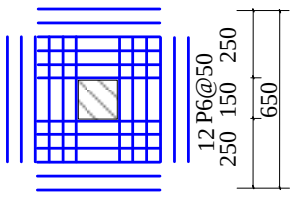

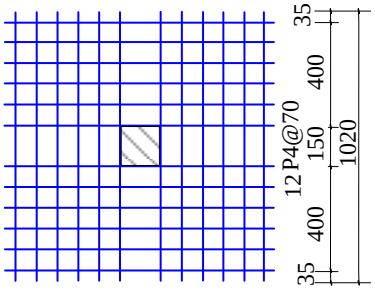

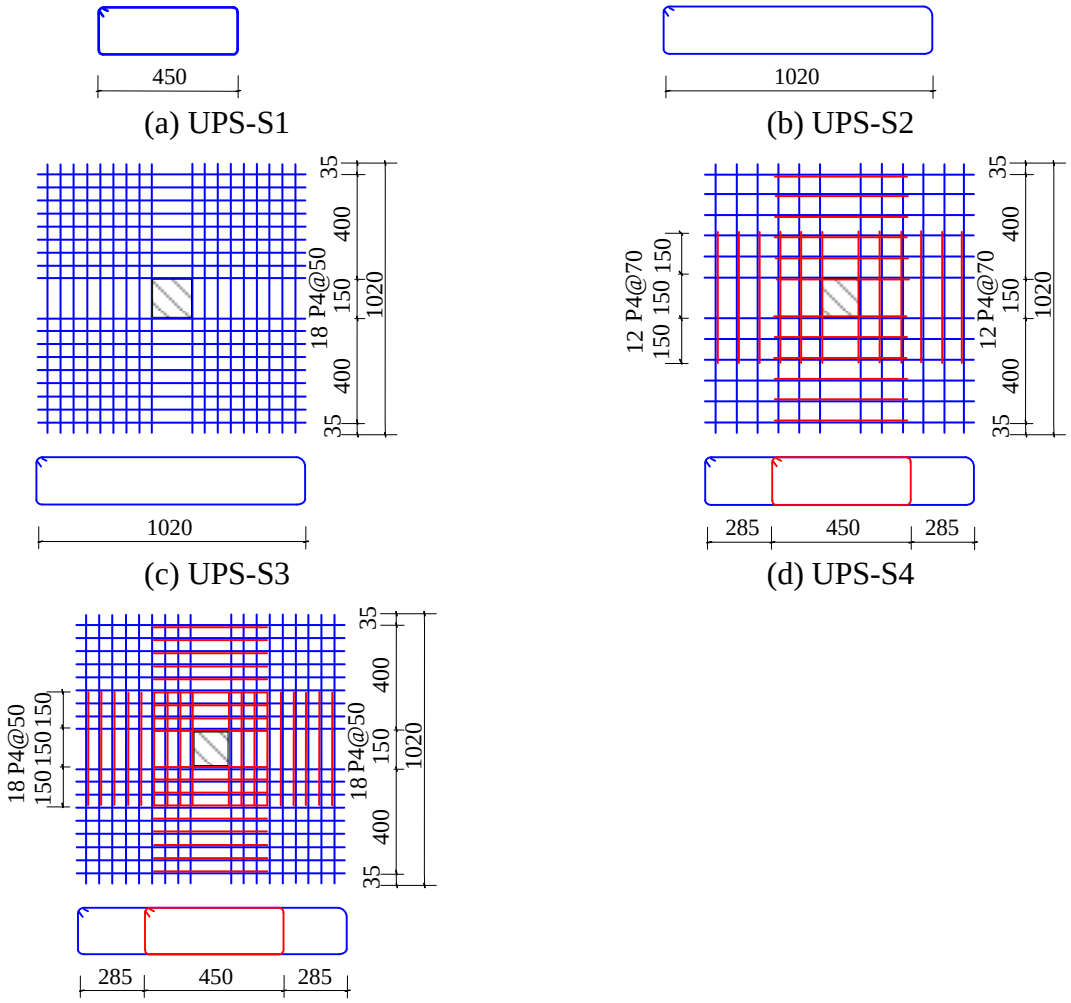

Fig. 18 Stirrup layouts for UPS-SI (I=1 to 5) specimens (unit: mm)

The load-displacement responses of the ten joint models are displayed in Fig. 19, together with those of USP-S and DPS-S. In Table 7, the displacements and the load resistances of these models at the critical points in the punching and post-punching stages are presented. The percentage increase and decrease in displacements and loads in relation to UPS-S/DPS-S are also included in the table. Noting that punching shear capacity is mainly regulated by the shear strengths of concrete and stirrups. Note also that post-punching strength is predominantly provided by the tensile mechanism exhibited in longitudinal reinforcements in the slab, and stirrups are effective to confine more reinforcing bars thereby contributing to the improvement in the post-punching strengths. Indeed, in all the ten joint models, increased quantity of stirrups or enlarged portion of concrete resisting shear forces have helped to enhance the confinement of the

joints. This in turn led to an increased level of stresses in the concrete, therefore their punching and post-punching strengths were notably enhanced (up to 26% and 17.3% respectively) but the corresponding deformations were much smaller (up to 33.9% and 27.1% respectively) compared to the UPS-S and DPS-S specimens.

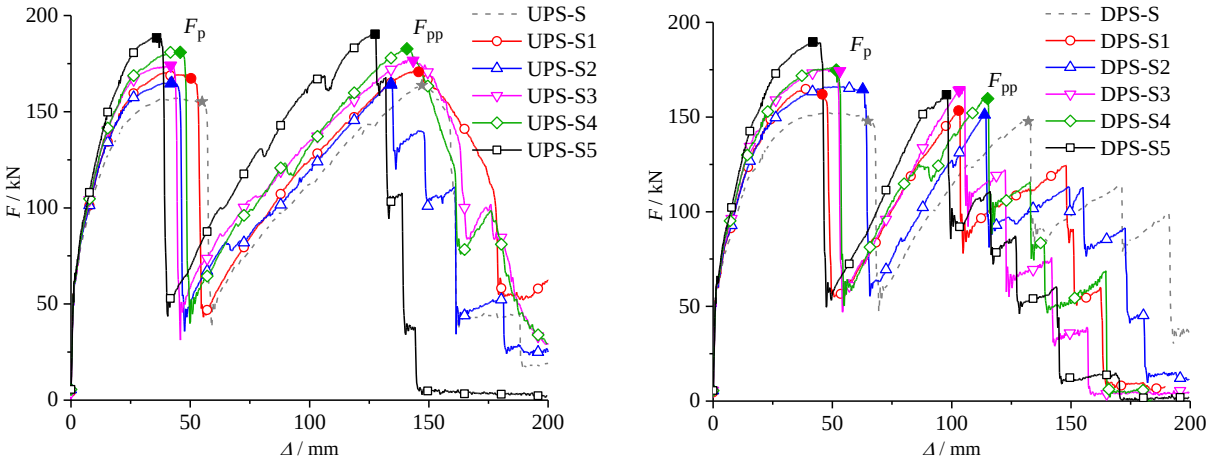

(a) UPS specimens (b) DPS specimens

Fig. 19 Load-displacement curves of UPS-SI and DPS-SI (I=1 to 5)

Table 7 Percentage variations of displacement and load resistance at the critical points

	Punching				Post-Punching			
	Displacement and percentage change (Δ_p, mm)		Load resistance and percentage change (F_p, kN)		Displacement and percentage change (Δ_{pp}, mm)		Load resistance and percentage change (F_{pp}, kN)	
UPS-S1	51	-7%	166	+8.4%	146	-3%	171	+5%
DPS-S1	42	-29.8%	164	+9.3%	103	-22%	153	+3.5%
UPS-S2	44	-19.3%	164	+6%	133	-11.3%	165	+1.2%
DPS-S2	63	-7.4%	164	+9.3%	114	-13.6%	152	+2%
UPS-S3	42	-24.5%	173	+10.9%	142	-4%	177	+9.3%
DPS-S3	51	-22%	174	+15.8%	105	-20.5%	164	+10%
UPS-S4	46	-14.8%	181	+13.8%	141	-4.7%	182	+11.7%
DPS-S4	51	-20.3%	174	+16%	115	-13.5%	159	+6.7%
UPS-S5	38	-33.9%	187	+22.7%	127	-15.3%	191	+17.3%
DPS-S5	44	-32.3%	189	+26%	97	-27.1%	161	+8%

Note: “+”and “-” represent the percentage increase and decrease compared to UPS-S/DPS-S, respectively.

In S2 specimens, the region confined by the stirrups was enlarged and effective to increase the punching shear strengths (F_p) under small deformations, the average value of F_p of UPS-S2 and

DPS-S2 was 8% higher than that of UPS-S and DPS-S. Nevertheless, due to widened stirrup spacings, the improvement of the confinement effects to the longitudinal reinforcing bars was limited, thus the average post-punching strength (F_{pp}) only increased by 2%, relative to the S specimens. The stirrup ratios of S1 and S3 specimens were increased from the S and S2 specimens, respectively. In comparison to the S specimens, the punching and post-punching strengths of S1 specimens were increased by 9% and 4%, respectively, while the increases were 13% and 10% in S3 specimens. This suggests that increased amount of stirrups can markedly improve the punching shear strength, whereas the post-punching strength is mainly regulated by the load resistant capacity contributed by the slab longitudinal reinforcements. Note that the confinements to these rebars were enhanced in S3 specimens, hence a significant increase in their post-punching strengths as well. Four-legged closed ties were adopted in S4 and S5 specimens, by adding internal stirrups to S2 and S3 specimens, respectively. Comparing to the S specimens, S4 had 15% and 9% increases in the punching and post-punching strengths, respectively; these increases were 24% and 13%, respectively, in S5 specimens.

As illustrated in Fig. 19b for the DPS specimens, when their load resistances reached F_{pp}, a stepwise decline was observed and all the values of F_{pp} were lower than the corresponding values of F_p. This is because the column stub was loaded downward, the concrete near the top reinforcing bars (IRs for UPS, FRs for DPS) sustained large compressive stresses. For the DPS specimens, the reinforcing bars at the slab top were FRs, of higher reinforcement ratio relative to the rebars at the same position in the UPS specimens (refer to Fig. 3b), therefore larger shear stresses were developed in the concrete core. With increased amount of stirrups, severer shear failure occurred at the concrete core, which reduced the support to the top reinforcements. Therefore, in the DPS specimens, confinement to FRs at the slab top was dramatically declined, causing successive drops in load resistance.

In general, with increased quantity of stirrups, the load resistances of the joint models were enhanced but the deformation capacities were lowered. The S5 specimens had the largest number of stirrups and were most effective to confine the slab longitudinal reinforcements. Hence the improvements to their punching and post-punching strengths were the most significant compared to the other joint models. However, overly supplied stirrups unfortunately promoted the

brittleness and decreased the deformation capacities of S5 specimens. Comparing to S4 specimens with a similar stirrup layout, the punching and post-punching strengths of S5 specimens were increased by 6% and 3%, respectively, while their corresponding deformation capacities were reduced by 15% and 13%, respectively. This implies that although four-legged closed ties were effective in improving the punching and post-punching strengths like in S4, there is little room for further improvement in load resistance by adding more stirrups like in S5. In addition, too many stirrups also made the joints more brittle which accelerated the punching shear failure. Moreover, comparison of the failure modes between S and S4 specimens (in Fig. 20) indicates that placing four-legged closed ties over a larger area was able to alleviate the joint damage. The damage zone was confined within the area where the stirrups were located. Therefore, if such a reinforcement configuration was adopted in a flat plate structure, damage propagation to the remaining part of the slab and disproportionate collapse of the entire structure could be prevented. As described above, reinforcement strengthening configurations analogous to those in S4 specimens are recommended to effectively enhance the structural performance with balanced load resistance and deformation capacity.

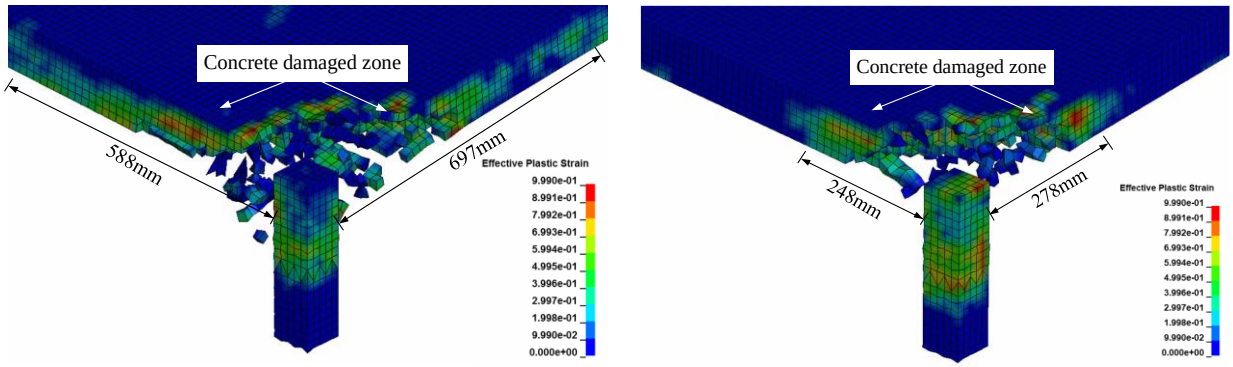

(a) DPS-S (b) DPS-S4

Fig. 20 Damaged concrete zone of DPS-S and DPS-S4

5.2 Effects of ring beams

In view of the UPS-R and DPS-R tests, care must be taken in designing the inner dimension of the ring beams, so as not to lower the punching shear strength on its inner edge, which may potentially create a vulnerable punching region between the column face and the ring beams. To demonstrate the effect of different ring beam configurations, two more models with the inner

edges of the embedded ring beams aligning with the column faces were designed based on UPS-R and DPS-R, and named as UPS-R1/DPS-R1 (Fig. 21a). The punching shear strengthens of the R1 models were further enhanced in that the applied load was resisted by the column and ring beams as an integral component. Furthermore, UPS-R2/DPS-R2 models (Fig. 21b) with an additional middle ring beam were also created based on the R1 models. The numerical simulation results of the four additional ring beam models (UPS-R1, DPS-R1, UPS-R2, DPS-R2) are presented in Fig. 22, along with those of UPS-R and DPS-R. In Table 8, the critical punching shear and post-punching deformations (Δ_p and Δ_{pp}, respectively) and strengths (F_p and F_{pp}, respectively) of the R1 and R2 models are given. The percentage values in the table denote either increased (+) or decreased (–) magnitudes in displacements and strengths compared to UPS-R/DPS-R.

In DPS-R1 and DPS-R2, the punching shear strengths enhanced moderately, while their post-punching deformation capacities and strengths improved remarkably by at least 10%, in relation to DPS-R. Furthermore, after the first punching shear failure, the load resistance in DPS-R1 and DPS-R2 increased steadily without the second punching-like load drop (Fig. 22).

Whereas for UPS-R1 and UPS-R2, no notable improvements were observed in the load resistance at both punching and post-punching stages, and the second punching-like drops in resistance still existed, similar to that in UPS-R. Note that the second load drop was more significant in the UPS-R test specimen, that was probably due to the 27% lower concrete strength of UPS-R compared to that of DPS-R (Table 2). In addition, the concrete parameters applied to UPS-R1/R2 and DPS-R1/R2 were consistent with those in UPS-R and DPS-R, respectively, which resulted in the reinforcement configurations contributed only limited shear strength prior to the shear failure of concrete in UPS-R1/R2.

To eliminate the concrete strength effect, the UPS-R2R model was also created based on UPS-R2, with the same concrete strength as DPS-R2. The simulation results are given in Fig. 23. The load-displacement response of UPS-R2R suggests that its punching shear failure was delayed compared to UPS-R2, which means that concrete strength makes a positive impact to further enhance the efficiency of the ring beam strengthening method. As shown in Fig. 23, having the

same concrete strength, similar trends were observed for UPS-R2R and DPS-R2 before punching shear failure. However, at the post-punching stage, the structural stiffness (the slope of post-punching stage in Fig. 23) in UPS-R2R was 112% higher than that in DPS-R2, suggesting that the reinforcing bars in UPS-R2R exhibited larger tensile stresses within a short period of time. With the tensile stresses developed in the rebars of UPS-R2R, the concrete was unable to provide sufficient confinement to those largely deformed rebars, therefore that load resistance could not increase anymore. It indicates that the concrete constraints could influence the performance of ring beams at the post-punching stage. The main propose of UPS-R2R is to delay the occurrence of punching shear failure when the inner edges of the embedded ring beams align with the column faces. In this regard, the embedded ring beams should be treated as an effective method to prevent punching shear failure and subsequent progressive collapse.

In other words, both stirrup and ring beam configurations enable more slab reinforcements to participate in resisting the applied loads. In the strengthened specimens/models, the differences in terms of the damage patterns, load resistances and deformations between the UPS and DPS directions were alleviated, owing to the stirrup confinement. As for the enhanced performance, double stirrups (four-legged closed ties) could effectively ease the joint damage and enhance both punching shear and post-punching strengths. Placing the embedded ring beams immediately next to the column eliminated premature punching shear failure and contributed to the considerably improved post-punching deformation and resistant capacities in the DPS models. Furthermore, the ring beam strengthening method also indicates that the enhanced performance was affected by the concrete strength as well.

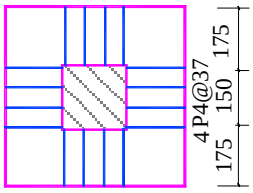

(a) UPS-R1/DPS-R1

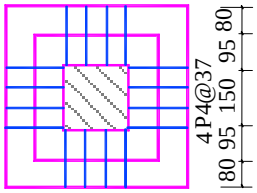

(b) UPS-R2/DPS-R2

Fig. 21 Additional R1 and R2 models with different stirrup layouts in ring beams (unit: mm)

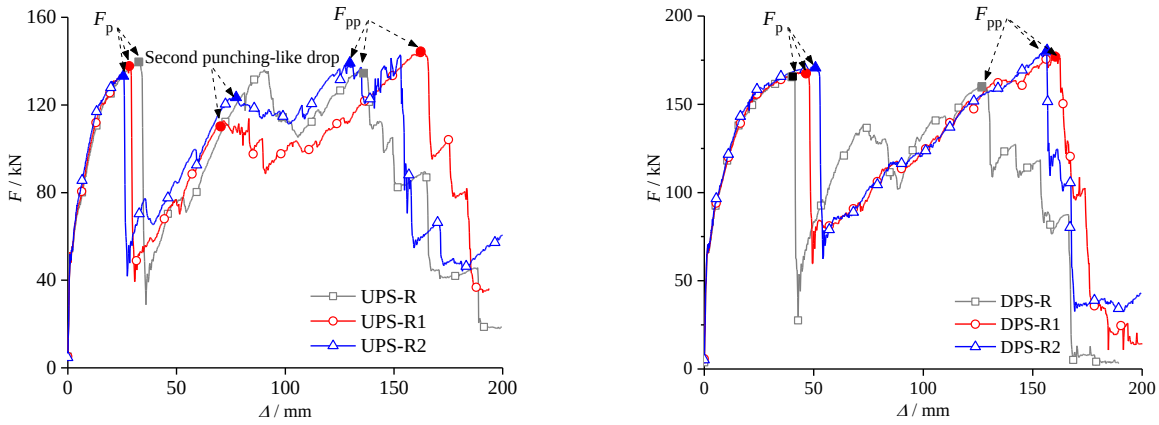

(a) UPS Series (b) DPS Series

Fig. 22 Load-displacement curves of UPS and DPS series

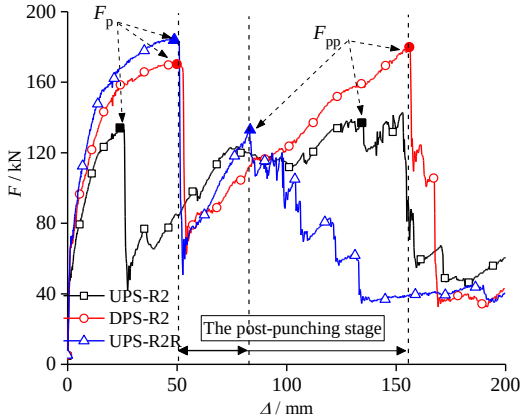

Fig. 23 Load-displacement curves of UPS-R2, DPS-R2 and UPS-R2R

Table 8 Percentage variations of displacement and load resistance at critical points

	Punching				Post-Punching			
	Displacement and percentage change (Δ_p, mm)		Load resistance and percentage change (F_p, kN)		Displacement and percentage change (Δ_{pp}, mm)		Load resistance and percentage change (F_{pp}, kN)	
UPS-R1	28	-12%	136	-2%	163	+21.6%	143	+6%
DPS-R1	47	+20%	168	+1%	160	+26%	177	+11%
UPS-R2	25	-21%	133	-4%	129	-4%	138	+2%
DPS-R2	51	+30%	170	+2%	156	+22%	180	+13%

Note: “+”and “-” represent the percentage increase and decrease compared to UPS-R/DPS-R, respectively.

6. Conclusion

(1) At the punching stage, punching shear failure happened twice in the ring beam specimens UPS-R and DPS-R, thereby the deformation and strength improvements were not as remarkable as those in the stirrup specimens UPS-S and DPS-S. At the post-punching stage, in comparison to UPS/DPS, the displacements in UPS-S/DPS-S and UPS-R/DPS-R were increased by 25% and 32% on average, along with the average strength improvements of 64% and 50%, respectively.

(2) The finite element models were validated by comparing the critical points of deformation and strength at the punching and post-punching stages, with less than 10% deviations. The experimental failure modes of the joints were well predicted, including severe concrete spalling, excessively deformed rebars, cracking and spalling of concrete, large rotation of reinforcing bars, punching shear failure around the column stub, as well as cracks forming two circular rings at the slab bottom.

(3) For the joints strengthened by stirrups, before punching shear failure, stirrups and concrete together exhibited large shear capacities to resist the applied load. While at the post-punching stage, the applied load was prominently resisted by the slab longitudinal reinforcements confined by the stirrups. A rational arrangement of four-legged closed stirrups (UPS-S4 and DPS-S4) is the most effective, in that it has not only lessened the failure of the joints, but also increased the punching and post-punching strengths by 15% and 9%, comparing to UPS-S/DPS-S, respectively.

(4) For the joints strengthened by embedded ring beams, placing the ring beam inner edges aligned with the column faces can prevent premature punching shear failure, which is recommended for engineering design. The strengthening efficiency of the ring beam configurations also depends on the constraints provided by the concrete.

Acknowledgements

The authors are grateful for the financial support received from the National Key Research and Development Program of China (No. 2019YFC1511000), the National Natural Science

Foundation of China (No. 51578018) and the Australian Research Council through an ARC Discovery Project (DP150100606).

References

1. N.J. Gardner, J. Huh, L. Chung, Lessons from the Sampoong department store collapse. Cem. Concr. Compos. 24 (6) (2002) 523-529.

2. A. Muttoni, M.F. Ruiz, A. Fürst, Structural safety of parking garages. Zürich: Swiss Society of Engineers and Architects. 105 (2008).

3. J. Schellhammer, N.J. Delatte, P.A. Bosela, Another look at the collapse of Skyline Plaza at Bailey's Crossroads. Virginia, J. Perform. Constr. Fac. 27 (3) (2012) 354-361.

4. F.H. Ma, B.P. Gilbert, H. Guan, H.Z. Xue, X.Z. Lu., Y. Li, Experimental study on the progressive collapse behaviour of RC flat plate substructures subjected to corner column removal scenarios. Eng. Struct. 180 (2019) 728-741.

5. F.H. Ma, B.P. Gilbert, H. Guan, H.Z. Xue, X.Z. Lu., Y. Li, Experimental study on the progressive collapse behaviour of RC flat plate substructures subjected to edge-column and edge-interior-column removal scenarios. Eng. Struct. 209 (2020) 110299.

6. K. Qian, B. Li, Load-resisting mechanism to mitigate progressive collapse of flat slab structures. Mag. Concr. Res. 67 (7) (2015) 349-363.

7. W.J. Yi, Q.F. He, Y. Xiao, S.K. Kunnath, Experimental study on progressive collapse-resistant behavior of reinforced concrete frame structures. ACI Struct. J. 105 (4) (2008) 433-439.

8. J.M. Russell, J.S. Owen, I. Hajirasouliha, Experimental investigation on the dynamic response of RC flat slabs after a sudden column loss. Eng. Struct. 99 (2015) 99 28-41.

9. N.M. Hawkins, D. Mitchell, Progressive collapse of flat plate structures. ACI J. 76 (1979) 775-808.

10. K.K. Choi, J.C. Kim, Nonlinear model simulating load-deformation relationship of flat plate structures. Eng. Struct. 85 (2015) 26-35.

11. Y. Tian, J.O. Jirsa, O. Bayrak, Widianto, J.F. Argudo, Behavior of slab-column connections of existing flat-plate structures. ACI Struct. J. 105 (6) (2008) 561-569.

12. T.H.-K. Kang, J.W. Wallace, Punching of reinforced and post-tensioned concrete slab-column connections. ACI Struct. J. 103 (4) (2006) 531-540.

13. A. Muttoni, Punching shear strength of reinforced concrete slabs without transverse

reinforcement. ACI Struct. J. 105 (4) (2008) 440-450.
14. M. Navarro, S. Ivorra, F.B. Varona, Parametric computational analysis for punching shear in RC slabs. Eng. Struct. 165 (2018) 254-263.
15. General Service Administration (GSA). Alternate path analysis and design guidelines for progressive collapse resistance, Washington, D.C., (2016).
16. Department of Defense (DoD). Unified Facilities Criteria (UFC): Design of buildings to resist progressive collapse. Washington, D.C., (2016).
17. American Society of Civil Engineering (ASCE7-10). Minimum design loads for buildings and other structures. Reston (VA) (2010).
18. A.M. Shaaban, H. Gesund, Punching shear strength of steel fiber reinforced concrete flat plates. ACI Struct. J. 91 (3) (1994) 406-414.
19. A.L. Carvalho, G.S. Melo, R.B. Gomes, P.E. Regan, Punching shear in post-tensioned flat slabs with stud rail shear reinforcement. ACI Struct. J. 109 (4) (2011) 579-581.
20. T.X. Dam, J.K. Wight, Flexurally-triggered punching shear failure of reinforced concrete slab-column connections reinforced with headed shear studs arranged in orthogonal and radial layouts. Eng. Struct. 110 (2016) 258-268.
21. M.P. Ferreira, G.S. Melo, P.E. Regan, R.L. Vollum, Punching of reinforced concrete flat slabs with double-headed shear reinforcement. ACI Struct. J. 111 (2) (2014) 363-374.
22. R. Cantone, M.F. Ruiz, J. Bujnak, A. Muttoni, Enhancing punching strength and deformation capacity of flat slabs. ACI Struct. J. 116 (5) (2019).
23. M.F. Ruiz, A. Muttoni, J. Kunz, Strengthening of flat slabs against punching shear using post-installed shear reinforcement. ACI Struct. J. 107 (4) (2010) 434-442.
24. L. Nguyen-Minh, M. Rovňák, T. Tran-Ngoc, T. Le-Phuoc, Punching shear resistance of post-tensioned steel fiber reinforced concrete flat plates. Eng. Struct. 45 (2012) 324-337.
25. A.P. Caldentey, P.P. Lavaselli, H.C. Peiretti, F.A. Fernández, Influence of stirrup detailing on punching shear strength of flat slabs. Eng. Struct. 49 (2013) 855-865.
26. D.M.V. Faria, V.J.G. Lucio, A.P. Ramos, Post-punching behaviour of flat slabs strengthened with a new technique using post-tensioning. Eng. Struct. 40 (2012) 383-397.
27. L. Keyvani, M. Sasani, Y. Mirzaei, Compressive membrane action in progressive collapse resistance of RC flat plates. Eng. Struct. 59 (2014) 554-564.
28. M.Z. Diao, Y. Li, H. Guan, X.Z. Lu, H.Z. Xue, Z.D. Hao, Post-punching mechanisms of

slab-column joints under upward and downward punching actions. Mag. Concr. Res. 2021, 73(6) 302-314.
29. Y.F. Zhang, J.H. Zhao, C.S. Cai, Seismic behavior of ring beam joints between concrete-filled twin steel tubes columns and reinforced concrete beams. Eng. Struct. 39 (2012) 1-10.
30. P. Pan, A. Lam, X.C. Lin, Y.X. Li, L.P. Ye, Cyclic loading tests and finite element analyses on performance of ring beam connections. Eng. Struct. 56 (2013) 682-690.
31. Q.J. Chen, J. Cai, A.B. Mark, X.P. Liu, Z.L. Zuo, Seismic behaviour of a through-beam connection between concrete-filled steel tubular columns and reinforced concrete beams. Eng. Struct. 80 (2014) 24-39.
32. AS 3600. Australian standard: concrete structures. Standards Association of Australia, Sydney, Australia, 2018.
33. GB 50010-2010. Code for design of concrete structures. Beijing: China Architecture & Building Press, 2010.
34. R. Park, W. L Gamble, Reinforced concrete slabs. John Wiley& Sons, 1999.
35. H.Z. Xue, H. Guan, B.P. Gilbert, X.Z. Lu, Y. Li, Simulation of punching and post-punching shear behaviours of RC slab-column connections. Mag. Concr. Res. (2020) 1-16.
36. A.T. Pham, N.S. Lim, K.H. Tan, Investigations of tensile membrane action in beam-slab systems under progressive collapse subject to different loading configurations and boundary conditions. Eng. Struct. 150 (2017a) 520-536.
37. A.T. Pham, K.H. Tan, J. Yu, Numerical investigations on static and dynamic responses of reinforced concrete sub-assemblages under progressive collapse. Eng. Struct. 149 (2017b) 2-20.
38. J. Yu, L.Z. Luo, Y. Li, Numerical study of progressive collapse resistance of RC beam-slab substructures under perimeter column removal scenarios. Eng. Struct. 159 (2018) 14-27.
39. Y.H. Weng, K. Qian, F. Fu, Q. Fang, Numerical investigation on load redistribution capacity of flat slab substructures to resist progressive collapse. J. Build. Eng. 29 (2020) 101109.
40. K. Qian, Y.H. Weng, B. Li, Impact of two columns missing on dynamic response of RC flat slab structures. Eng. Struct. 177 (2018) 598-615.
41. H.Z. Xue, H. Guan, B.P. Gilbert, X.Z. Lu, Y. Li, Comparative and parametric studies on behavior of RC-flat plates subjected to interior-column loss. J. Struct. Eng. 146 (9) (2020), 04020183.

42. CEB-FIP Euro-International Committee for Concrete/International Federation for Prestressing. 1993. Model code 1990. MC 1990. Lausanne.

Appendix 1 The parameter details in CSCM

Notation	Description	Formula
SHEAR	Elastic parameters	$G=\frac{E}{2(1+\gamma)}$
BULK		$K=\frac{E}{3(1-2\gamma)}$
Poisson's Ratio		0.2
Young's Modulus		$E=21.5\times10^3(\frac{f_c^{'}}{10})^{1/3}$
ALPHA	Triaxial compression, torsion and extension	$\alpha=-0.003(f_c^{'})^2+0.3169747f_c^{'}+7.7047$
THETA		$\theta=\frac{1.3216}{10^5}(f_c^{'})^2+\frac{2.3548}{10^3}f_c^{'}+0.2140058$
LAMDA		10.5
BETA		$\beta=\frac{1.929}{10^2}$
ALPHA1		0.74735
THETA1		$\theta=-\frac{3.8859}{10^7}(f_c^{'})^2-\frac{3.9317}{10^6}f_c^{'}+\frac{1.5820}{10^3}$
LAMDA1		0.17
BETA1		$\beta=\frac{-1.9972}{10^5}(f_c^{'})^2+\frac{2.2655}{10^4}f_c^{'}+\frac{8.1748}{10^2}$
ALPHA2		0.66
THETA2		$\theta=\frac{-4.8697}{10^7}(f_c^{'})^2-\frac{1.8883}{10^6}f_c^{'}+\frac{1.8822}{10^3}$
LAMDA2		0.16
BETA2		$\beta=-\frac{1.9972}{10^5}(f_c^{'})^2+\frac{2.2655}{10^4}f_c^{'}+\frac{8.1748}{10^2}$
R	Cap surface parameters	5.0
X_0		$X_0=\frac{8.769178}{10^3}(f_c^{'})^2-\frac{7.3302306}{10^2}f_c^{'}+84.85$
W		0.05
D1		$D1=\frac{2.5}{10^4}$

D2		$D2=\frac{3.492}{10^7}$
B	Damage parameters for strain softening of the concrete solid elements	10.0
D		0.1
G_{fs}		$G_{fs}=C_{ms}G_{F0}\left(\frac{f_c}{10}\right)^{0.7}$
G_{ft}		G_{fs}
G_{fc}		$100G_{fs}$
PWRC		5.0
PWRT		1.0
PMOD		0.0